Structural, Microchemistry, and Hydrogenation Properties of $TiMn_{0.4}Fe_{0.2}V_{0.4}$, $TiMn_{0.1}Fe_{0.2}V_{0.7}$ and $Ti_{0.4}Zr_{0.6}Mn_{0.4}Fe_{0.2}V_{0.4}$ Metal Hydrides

E. D. Koultoukis[1,2,3,*], S. S. Makridis[1,3], L. Röntzsch[4], E. Pavlidou[2],
A. Ioannidou[3], E. S. Kikkinides[3], and A. K. Stubos[1]

[1] *Institute of Nuclear Technology and Radiation Protection, NCSR "Demokritos,"
Ag. Paraskevi, Athens, GR 15310, Greece*
[2] *Department of Physics, Aristotle University of Thessaloniki, Thessaloniki, GR 54124, Greece*
[3] *Department of Mechanical Engineering, University of Western Macedonia,
Bakola and Sialvera, Kozani, GR 50100, Greece*
[4] *Fraunhofer Institute for Manufacturing Engineering and Applied Materials Research,
Dresden, DE 01277, Germany*

In this work, TiFe-based alloys have been developed according to the stoichiometry $Ti_{1-x}A_xFe_{1-y}B_y$ (A ≡ Zr; B ≡ Mn, V). The hydrogen solubility properties have been investigated to develop dynamic hydrides of Ti-based alloys for hydrogen storage applications. The hydrogenation behavior of these alloys has been studied, and their hydrogen storage capacities and kinetics have been evaluated. Several activation modes, including activation at high temperatures under hydrogen pressure, have been attempted for the as-milled powders. In order to clarify the structural/microstructural characteristics, and chemical composition before and after hydrogenation, X-Ray Diffraction (XRD), EDAX—Mapping Analysis and Scanning Electron Microscopy (SEM), have been carried out for the samples. Modeling of the isotherms has been performed by using MATLAB programming. The maximum gravimetric density of 4.3 wt%, has been obtained on the sample with the BCC main phase. The calculated enthalpy of reaction (ΔH) is found to be about 4 kJ/mol.

Keywords: TiFe-Based Alloys, Rietveld Analysis, SEM Analysis, Hydrogen Absorption, Computer Simulation.

RESEARCH ARTICLE

1. INTRODUCTION

The limited supply of fossil fuels and their adverse environmental effects make it necessary to find renewable and clean energy sources. Of all the alternative fuels, hydrogen is now known to be a potential renewable substitute for petroleum for the future.[1] Hydrogen would be ideal as a synthetic fuel because, it has a very high energy content per unit mass, it is highly abundant and its oxidation product (water) is environmentally friendly. However, considerable difficulties exist associated with the efficient production and storage of hydrogen for automotive or other applications.[2] Among these, finding an economically viable and safe method of storing hydrogen on-board is the greatest hurdle.

Solid hydrogen storage using intermetallic compounds has been a field of intensive interest over the last decades and several investigations have been carried out to determine the fundamental properties of these materials, i.e., crystal structure, microchemistry, diffusivity, etc.[2,3] Besides hydrogen storage[1,4–7] (which is the main application targeted in this work) such systems can be potentially useful in a number of applications like hydrogen batteries,[8–11] heat pumps,[12–14] hydrogen isotopic separation,[15,16] gas compressors[17–19] and refrigerators.[20] Indeed, the hydriding/dehydriding kinetics of metal hydrides are relevant to the design and application of various metal hydride devices (cooling systems, power generators, batteries and automobiles).[21]

The relationship between the metal hydride concentration (C), temperature (T), and pressure (P) defines the technical reaction kinetics[22,23] and the performance of metal hydride cooling systems.[24,25] Therefore, the P-C-T correlation with experimental results is a key factor in any metal hydride system.[26]

*Author to whom correspondence should be addressed.

The AB-type intermetallics can store up to 1.8% hydrogen by weight with medium kinetics whereas the stability of the hydrides varies. Among AB intermetallics, the TiFe system has been studied for decades due to its moderate kinetics with relatively high equilibrium pressure (4–5 atm) at room temperature. The low storage capacity and O_2, H_2O, CO poisoning problems could not be solved for practical applications.[27] According to Thompson et al.,[28] TiFe has a CsCl-type structure which corresponds to Pm3m space group with a lattice parameter of 2.9789 Å. On the other hand, Miao et al.[29] have found that a V-based solid solution phase exists in such alloys, which is associated to the Im3m space group with a lattice parameter of 2.9650 Å.

The TiFe-based alloys are promising hydrogen storage materials, with low production cost and adequate (for stationary and portable applications) hydrogen capacity. However, they exhibit certain disadvantages such as, high hydrogenation pressure, high activation temperature, and large hysteresis.[30–33] Furthermore, these compounds react with hydrogen to form two hydrides, TiFeH and TiFeH2.

One promising way to improve TiFe properties, is by substituting Ti and Fe by other elements, while its inherent advantages remain the same.[34] Even so, there have been few reports on the substitution of titanium, rather than of iron in TiFe in order to improve the activation properties.[31] Therefore, it has been attempted to produce a sample by substituting Ti by Zr in TiFe-type intermetallic compounds.[31] After Ti is substituted by a small amount of Zr, the pressure plateau and hydrogen capacity decrease.[31] This addition of Zr, results to an alloy with interesting properties.[34] In general, the Ti based alloys are less stable than the Zr based alloys due to the lower atomic radius of Ti compared to Zr ($r_{Ti} = 140$ pm, $r_{Zr} = 160$ pm).[35]

In the present work, we have made an effort to develop new TiFe-based alloys, by substituting Ti and Fe with other elements. Properties and characteristics of the new alloys are discussed on the basis of structural, microchemistry and interstitial hydrogen absorption/desorption (IHAD) analysis.

2. EXPERIMENTAL PROCEDURE

High purity granules of titanium, manganese, iron, vanadium and zirconium have been used with respect to the stoichiometric proportion. Arc-melting has been employed for the development of bulk materials by repeated welding, under pure (99.999%) argon atmosphere.[36–38] The as-cast samples were 3 g of mass. The produced buttons have been cleaned in order to remove the poisoned surface of oxide films. A high energy planetary ball miller (RETSCH PM 400/2) has been used for the production of the microsized powder, under pure argon atmosphere. X-ray diffraction analysis of the alloys was carried out on the powders, at room temperature by using Cu-K$_\alpha$

radiation, in a SIEMENS D500 X-Ray diffractometer. Rietveld analysis has been performed on the XRD patterns with the use of the RIETICA software.[40] SEM/EDAX analysis has been performed for microchemistry and elementary mapping analysis. The pressure-composition-temperature (PCT) isotherms have been traced on the three samples via a high pressure, as high as 10 MPa, Sievert's-type volumetric apparatus. In addition, the hydrogenation/dehydrogenation kinetics and cycle stability of the sample TiMn$_{0.4}$Fe$_{0.2}$V$_{0.4}$ have been studied, using a Magnetic Suspension Balance (Rubotherm). In this latter equipment, hydrogen desorption and re-absorption, can be investigated at constant hydrogen pressures in the range from 1 to 20 MPa (flow-through mode), i.e., covering the operating pressure range of most PEM fuel cell systems. The MATLAB software has been used for the simulation of the resulting P-C-T curves.

3. EXPERIMENTAL RESULTS AND DISCUSSION

As shown in Figure 1, Rietveld analysis has been performed on the three samples. The main phase of the alloys is the V-based solid solution phase with a BCC structure which corresponds to Im3m space group. The hexagonal C14 Laves phase (MgZn$_2$-type of structure) and the cubic C15 Laves phase (MgCu$_2$-type of structure) have also been found as secondary phases. Some traces of C14 phase (a,b = 4.85740 Å, c = 8.06290 Å) at 8.86 wt% have been calculated through the analysis. The Zr-free samples have the characteristic BCC main phase. As Mn has been decreased and V has been increased, the C14 phase weight percentage has decreased. In the Zr-doped sample, the analysis has revealed three (at least) phases and the C14 amount has increased remarkably, deteriorating the BCC part crystallization. The C15 Laves phase coexists at
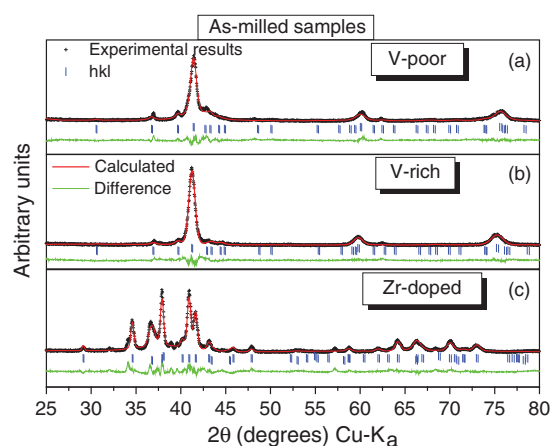
Fig. 1. Rietveld analysis of (a) TiMn$_{0.4}$Fe$_{0.2}$V$_{0.4}$, (b) TiMn$_{0.1}$Fe$_{0.2}$V$_{0.7}$, (c) Ti$_{0.4}$Zr$_{0.6}$Mn$_{0.4}$Fe$_{0.2}$V$_{0.4}$.

high concentrations (∼25 wt%). The V-rich sample seems to be an almost single phase alloy. As it has been expected from,[31] the V-poor sample (with higher C14 concentration) is associated to better HAD characteristics.

Table I summarizes the lattice parameters, unit cell volumes and phase percentages of $TiMn_{0.4}Fe_{0.2}V_{0.4}$, $TiMn_{0.1}Fe_{0.2}V_{0.7}$, and $Ti_{0.4}Zr_{0.6}Mn_{0.4}Fe_{0.2}V_{0.4}$, that have been calculated after the Rietveld refinement on the X-ray diffraction patterns. It has been reported that the hydrogen storage capacity of the hydrogen absorbing phase is affected by the unit cell volume.[39] The V-based solid solution phase itself can only absorb a small hydrogen amount, but its hydrogen absorption capacity can be greatly improved by the catalysis of the C14 Laves phase in alkaline solution. However, the hydrogen absorption capacity of the C14 Laves phase is lower than that of the V-based solid solution phase.[39] This is the reason why we have made more analysis on the first sample (V-poor), to discover the influence of the C14 Laves phase on the properties of the BCC solid solution and the hydrogen storage ability of the sample.

The Full Width at Half Maximum (FWHM) and the integral breadth (area of the peak divided by the maximum intensity) are often considered as a measure of the broadening of the diffraction peaks. If the FWHM of the reflections of a line profile, increases with the diffraction angle, the broadening is called isotropic otherwise it is termed as an anisotropic peak broadening (Figs. 2–4). This anisotropic line shape broadening is frequently observed in powder diffraction pattern and creates a serious difficulty for the Rietveld analysis.[41] It is a simple and well-defined number which can be used to compare the quality of images obtained under different observing conditions. Evidently, the peak broadening is isotropic for each sample and phase, and the Rietveld refinement is well done.

After the hydrogenation—dehydrogenation procedure, the grain size of the powders has been obviously affected and the decrease of the grain size can be identified by the peaks' broadening in the X-ray powder diffraction patterns, in Figure 5.

The SEM/EDAX analysis (Figs. 6–8) has shown that the alloys are multiphase systems. The metallographic examination of the microstructure indicates that the $TiMn_{0.4}Fe_{0.2}V_{0.4}$, $Ti_{0.4}Zr_{0.6}Mn_{0.4}Fe_{0.2}V_{0.4}$ alloys have three phases. Microchemistry examinations and mapping analysis by EDAX, as shown in Table II, reveal that the brighter regions are the matrix phase of Ti and V, while dark grey regions are phases of pure Ti, with a lack of Fe and Mn. The black spots at bottom left of the images are cavities that have resulted from the sample treatment process before an examination. For the Zr-doped sample, the darker regions are the matrix phase, while brighter regions are phases of pure Ti and Zr. These minor phases are not present in X-ray diffraction patterns of the Zr-free samples. The three not fitted small peaks in Figure 1(c), can be possibly explained by the detected non-uniformities, that are associated to the Zr (Table II—white region (3)).

As for Figure 7, it is easily palpable that the cyclic hydrogenation/dehydrogenation procedure affects the compact structure of the grains and cracks are beginning to appear. This is explained by the change of volume of the unit cell, as the hydrogen atoms are placed inside the cell, and the whole grain begins to expand. This effect is desirable in relation to the formation of new surfaces, but it has to be investigated, until what stage of fragmentation, this effect is positive, because this could result into an amorphous material.

For the activation and the hydrogen absorption/desorption measurements, a Sievert's-type volumetric apparatus has been used, in a layout like the one shown in Figure 9. All parts and connections as well as the container (whose maximum capacity is about 1 g of metal powder) are made of stainless steel. Around the container there is an electric heater, while the temperature is measured by a thermocouple. Before each measurement, this device vacuums every single part and uses helium in order to determine the volume of the specimen inside the container.

As shown in Figure 10 and as expected, the $TiMn_{0.1}Fe_{0.2}V_{0.7}$ alloy has faster hydrogenation kinetics at the beginning of hydrogenation when the hydrogen content is low. After 18—20 minutes, the container's pressure was stabilized for each pressure range (or there was no significant pressure drop, so we were moving to the next

RESEARCH ARTICLE

Table I. Structural characteristics of $TiMn_{0.4}Fe_{0.2}V_{0.4}$, $TiMn_{0.1}Fe_{0.2}V_{0.7}$, $Ti_{0.4}Zr_{0.6}Mn_{0.4}Fe_{0.2}V_{0.4}$ alloys.

Samples	Space group (No.)	Phase	Lattice parameters (Å) a	c	Cell volume ($Å^3$)	Phase abundance (wt%)	R_p	R_{wp}	χ^2
$TiMn_{0.4}Fe_{0.2}V_{0.4}$	Im3m	b.c.c.	3.0759		29.10584	81.23	13.213	17.667	2.443
	P63/mmc	C14	4.8767	8.0581	191.63936	18.77			
$TiMn_{0.1}Fe_{0.2}V_{0.7}$	Im3m	b.c.c.	3.0886	—	29.46354	91.14	11.279	11.279	2.464
	P63/mmc	C14	4.8574	8.0629	190.23876	8.86			
$Ti_{0.4}Zr_{0.6}Mn_{0.4}Fe_{0.2}V_{0.4}$	Im3m	b.c.c.	3.3409	—	37.28983	30.11	11.978	16.171	4.793
	P63/mmc	C14	5.1811	8.3834	151.31389	45.37			
	Fd3m	C15	6.9076	—	329.59570	24.53			

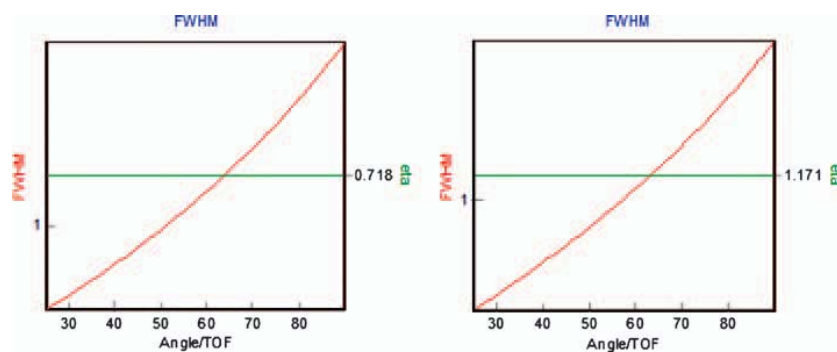*R_p, the pattern factor, R_{wp}, the weighted pattern factor, χ^2, the goodness of fit

Fig. 2. Full width half maximum of theoretical Rietveld analysis of $TiMn_{0.4}Fe_{0.2}V_{0.4}$ alloy, for the Im3m phase and the C14 Laves phase, respectively.

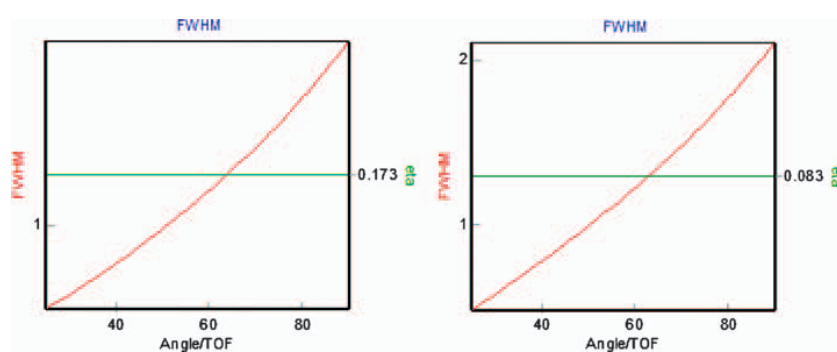**Fig. 3.** Full width half maximum of theoretical Rietveld analysis of $TiMn_{0.1}Fe_{0.2}V_{0.7}$ alloy, for the Im3m phase and the C14 Laves phase, respectively.
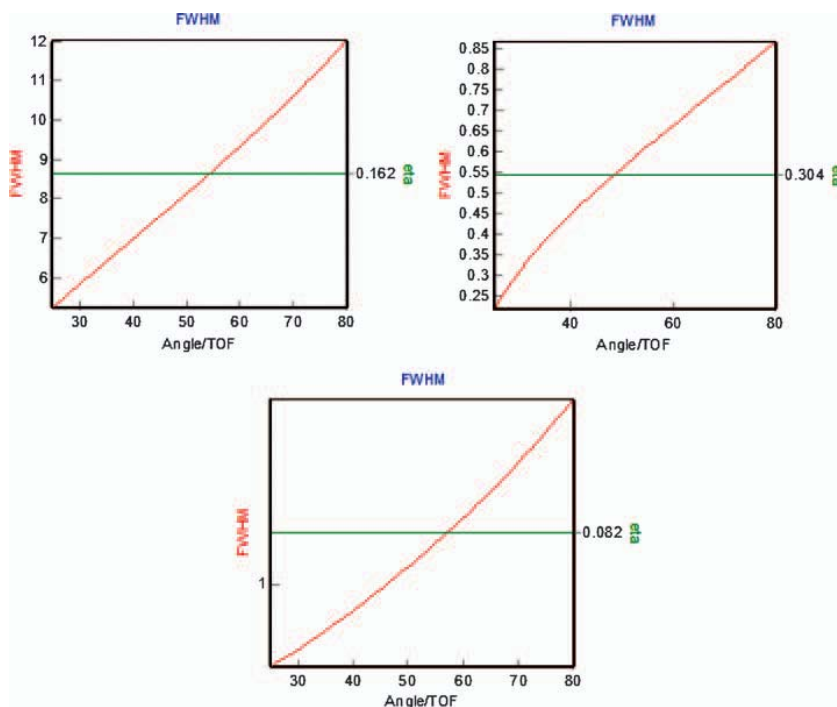

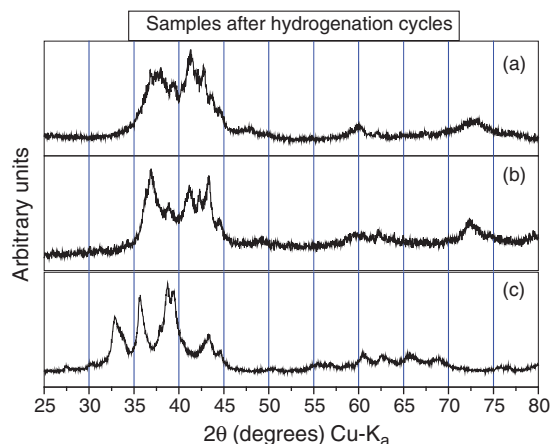**Fig. 4.** Full width half maximum of theoretical Rietveld analysis of $Ti_{0.4}Zr_{0.6}Mn_{0.4}Fe_{0.2}V_{0.4}$ alloy, for the Im3m phase, the C14 and C15 Laves phase, respectively.

4

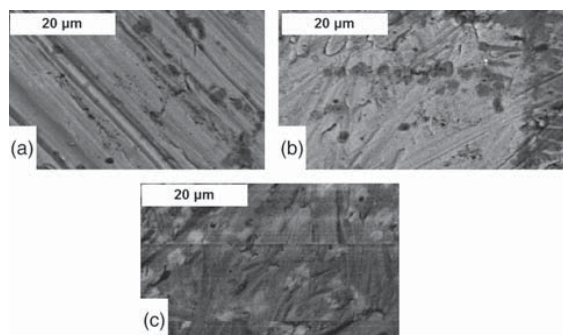**Fig. 5.** X-ray powder diffraction patterns of (a) $TiMn_{0.4}Fe_{0.2}V_{0.4}$-H, (b) $TiMn_{0.1}Fe_{0.2}V_{0.7}$-H, (c) $Ti_{0.4}Zr_{0.6}Mn_{0.4}Fe_{0.2}V_{0.4}$-H alloys.

Fig. 7. SEM images of $TiMn_{0.4}Fe_{0.2}V_{0.4}$ (a) before and (b), (c) after hydrogenation.

pressure step), which means that the material has more or less fast kinetics.
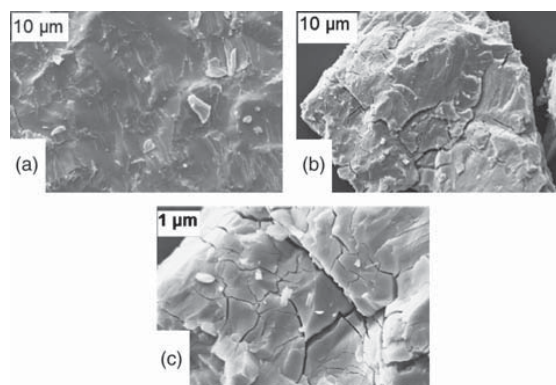
Figure 11, shows the effect of hydrogen absorption as a function of time and temperature. The biggest slope change has been obtained after freezing the sample container in ice.

Due to the similar stoichiometry of the three compounds, it was decided that the measurements (Fig. 12) would be conducted under different conditions, in order to study different aspects of their reaction. Moreover, the best reaction between these three alloys, was found to be that of the $TiMn_{0.4}Fe_{0.2}V_{0.4}$, and thus this alloy was chosen for further hydrogen absorption/desorption measurements using a Magnetic Suspension Balance.

Figure 12(a) shows a comparison of the isotherms of $TiMn_{0.4}Fe_{0.2}V_{0.4}$ at 303 K after activation procedures. The activation has a major influence on the hydrogenation/dehydrogenation behavior, and the activation procedure for every measurement is described below. The first measurement has been performed on the as-milled sample, after the laundry process under 2 MPa of hydrogen
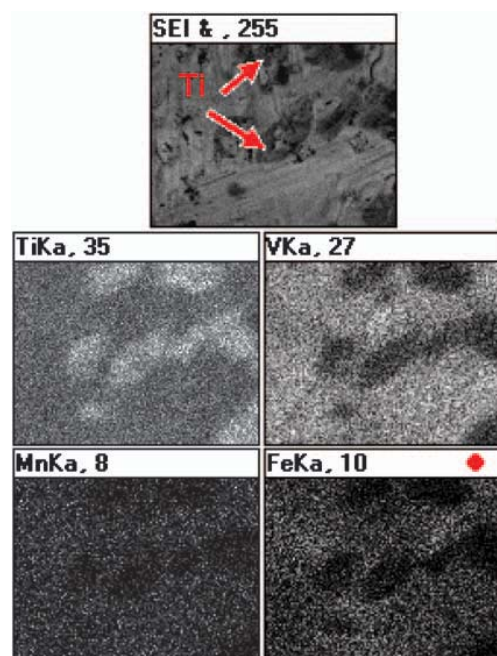
at 523 K. Vacuum has been applied for about a half hour, and the whole procedure was repeated once more before the measurement. The reason why this sample absorbs hydrogen at the dehydrogenation process seems to be that not all surfaces are clean and activated, even after reaching the high pressure. One important problem here is the remaining hydrogen in the material, which means that a stable metal hydride has been created at 303 K.

The activation of the sample consists of a heat treatment at 523 K and a hydrogen pressure of about 3 MPa. The next step is to let the alloy to absorb hydrogen while its temperature is decreased to 273 K. Vacuum has been applied at

Fig. 6. SEM images of (a) $TiMn_{0.4}Fe_{0.2}V_{0.4}$ (b) $TiMn_{0.1}Fe_{0.2}V_{0.7}$ and (c) $Ti_{0.4}Zr_{0.6}Mn0_{.4}Fe_{0.2}V_{0.4}$.

Fig. 8. Mapping images of $TiMn_{0.1}Fe_{0.2}V_{0.7}$.

Table II. Elemental and atomic stoichiometry of the $TiMn_{0.4}Fe_{0.2}V_{0.4}$, $TiMn_{0.1}Fe_{0.2}V_{0.7}$, $Ti_{0.4}Zr_{0.6}Mn_{0.4}Fe_{0.2}V_{0.4}$ hydrogen storage alloys.

$TiMn_{0.4}Fe_{0.2}V_{0.4}$ (1), $TiMn_{0.1}Fe_{0.2}V_{0.7}$ (2), $Ti_{0.4}Zr_{0.6}Mn0_{4}Fe_{0.2}V_{0.4}$ (3)

	Matrix			Dark region			White region		
	Weight %								
	(1)	(2)	(3)	(1)	(2)	(3)	(1)	(2)	(3)
Ti	50.32	48.58	13.79	48.29	91.55	—	—	—	15.00
V	19.22	32.65	19.28	25.24	7.36	—	—	—	8.52
Mn	16.33	4.60	10.74	15.66	0.36	—	—	—	4.92
Fe	13.70	14.17	10.93	10.56	0.72	—	—	—	4.63
Zr	—	—	45.26	—	—	—	—	—	66.93

303 K for about 18 hrs. This second measurement shows clearly how the activation cycle affected the behavior of the material. It seems that a stable hydride has been created at the temperature of 523 K, and thus the alloy cannot reversibly absorb hydrogen, since it has already absorbed some amount during activation.

The third measurement has been performed after two activation cycles. In the previous as well as in this measurement, there is a little amount of remaining hydrogen in the material and this is the major advantage of the activation process on the material. However, in this case, the maximum hydrogen concentration has been reduced, which probably means that there is a stable hydride remaining from previous measurements.

The isotherm of hydrogen absorption-desorption for the fine powdered $TiMn_{0.1}Fe_{0.2}V_{0.7}$ sample at 393 K is shown in Figure 12(b). As temperature increases, the pressure plateau increases as well, and the hydrogen storage capacity is reduced, as expected.[31] The typical TiFe-type of compounds has a pressure plateau at about 0.8–1 MPa at room temperature and the slope has increased as other dopants (Al) substitutes Fe.[39] There is no presence of pressure plateau in the P-C-T curve at 393 K, as it has been expected observed in other relevant compositions.

Figure 12(c) shows a comparison of the hydrogen pressure—composition isotherms of $Ti_{0.4}Zr_{0.6}Mn_{0.4}Fe_{0.2}V_{0.4}$ at 273 K with different activation modes. In this case too, the measurement has been performed with the sample

as—milled and the only preparation has been a laundry process under 4 MPa of hydrogen at 423 K. After the system had been stabilized, vacuum was applied for about a half hour, and the whole procedure was repeated once more before the measurement.

The activation of the sample for the second measurement, has been carried out at 473 K to 273 K and at a hydrogen pressure of 3 MPa. After that, vacuum has been applied at 473 K for approximately 20 h. The conclusion from these two last measurements is that the activation process deteriorates albeit at a small extent, the hydrogen related properties of the material. This might be justified by the addition of Zr, which partly solves the poisoning problems of the metal hydride. For this sample, the maximum concentration is small, as we expected, compared to the other samples, because of the presence of Zr.

For the measurements shown in Figures 13 and 14, the activation has been carried out at 523 K and at a pressure of 3–3.5 MPa, using different temperature variations versus time. After the activation, two different modes of dehydrogenation have been used. For the measurement of Figure 12, the dehydrogenation pressure was 0 MPa, while the dehydrogenation pressure of the measurement of Figure 13 varied from 0 MPa to 0.1 MPa, after each reversed cycle. The maximum absorbed hydrogen was
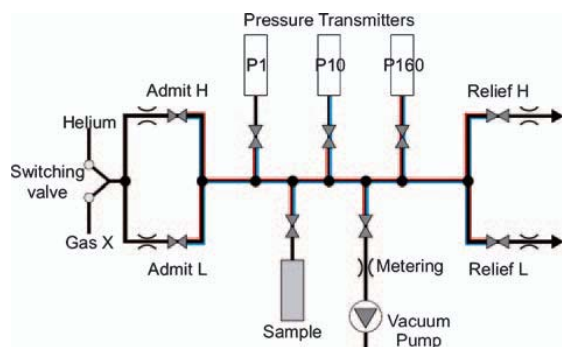
Fig. 9. Layout of the high pressure Sievert's type volumetric apparatus.
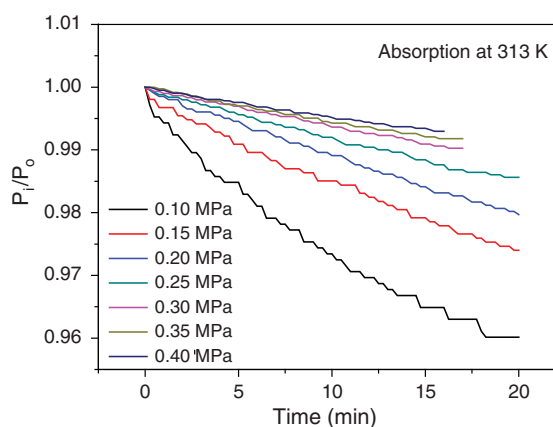
Fig. 10. Pressure kinetics of $TiMn_{0.1}Fe_{0.2}V_{0.7}$.

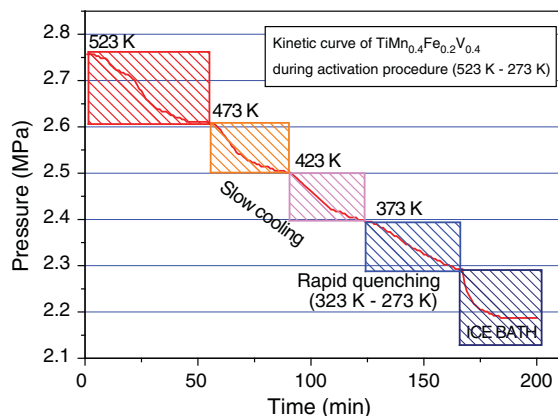**Fig. 11.** Pressure versus time, P(t), curve of $TiMn_{0.4}Fe_{0.2}V_{0.4}$ during activation.

Fig. 13. Hydrogenation/dehydrogenation kinetics of $TiMn_{0.4}Fe_{0.2}V_{0.4}$ (1).

about 4.3 wt%, but the amount of the desorbed hydrogen was about 1.5 wt%. We observe that there is a small but steady increase of the maximum concentration of hydrogen after each cycle, which is explained by the fragmentation of the material and the formation of new surfaces. Nevertheless, the desorbed hydrogen after each cycle is not too much, and this could be explained by the formation of stable hydrides during the activation at high temperatures. So, activation is really necessary, at least for these materials, but the question could be at what temperature is the activation more effective, in order to avoid formation of stable hydrides. However, this effect is reversible, as a great amount of hydrogen is desorbed when the temperature rises up again after the activation, as Figure 14 shows.

As shown in Figure 15, the absorption curves of the $TiMn_{0.4}Fe_{0.2}V_{0.4}$ alloy have been simulated with a 9th order polynomial, using the MATLAB software. Table II lists the fitting parameters for these two P-C-T isotherms. Figure 14
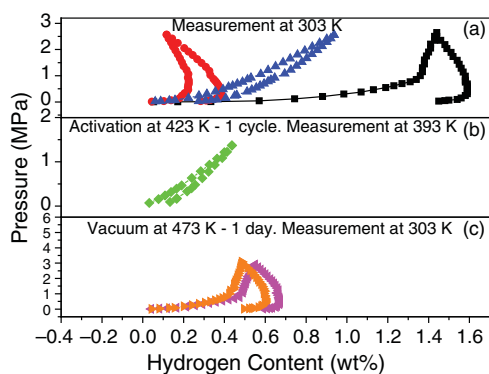
indicates very good agreement between the measurement and the model within the range of the pressure plateau. According to Payá et al.,[42] the polynomial fitting model is not expected to be sufficiently accurate with regard to the narrowing of the plateau region at high temperatures. It has to be noted that this model is valid only for the calculation of the equilibrium pressure, and it cannot be used inversely for the calculation of the metal hydride concentration.[38] The reaction enthalpy (ΔH) is the energy that the system rejects during hydrogen absorption (hydride formation) or needs in order for the hydrogen to be desorbed. The calculated reaction enthalpy ΔH from the fitted curve with a 9th order polynomial is presented in Table III, and the enthalpy resulting from the experimental data (slope of the line in the second part of Fig. 14) is 4587 $Jmol^{-1}$. This means that the error (percentage difference between the two values of ΔH) is only 15%, an acceptable range as reported in other cases.[38]

Fig. 12. P-C-T curves of (a) $TiMn_{0.4}Fe_{0.2}V_{0.4}$ (black: Vacuum at 523 K, red: Activation at 523 K - 1 cycle, blue: Activation at 523 K - 2 cycles), (b) $TiMn_{0.1}Fe_{0.2}V_{0.7}$, (c) $Ti_{0.4}Zr_{0.6}Mn_{0.4}Fe_{0.2}V_{0.4}$ (magenta: Measurement without activation, orange: Measurement after activation at 473 K - 1 cycle).
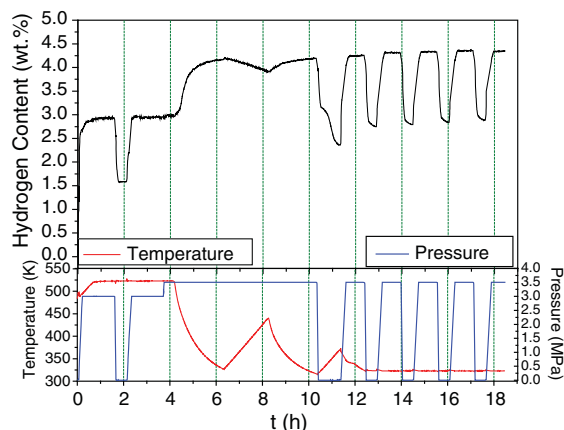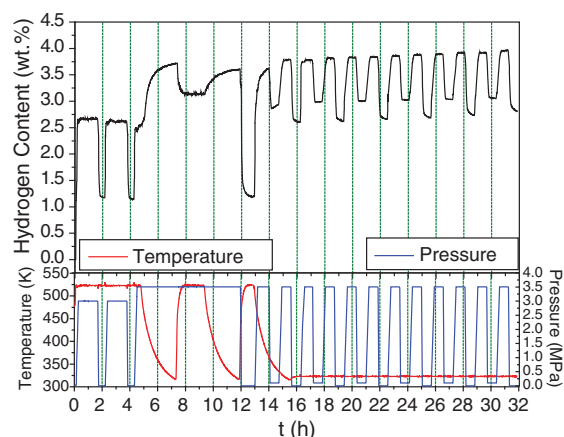

Fig. 14. Hydrogenation/dehydrogenation kinetics of $TiMn_{0.4}Fe_{0.2}V_{0.4}$ (2).

RESEARCH ARTICLE

Table III. Fitting parameters of the polynomial fitting method.

Parameters	$TiMn_{0.4}Fe_{0.2}V_{0.4}$	
T	30 °C	60 °C
T_{ref}	30 °C	
ΔH	3898 (Jmol^{-1}) (exp)	
	4587 (Jmol^{-1}) (calc)	
k0	0.00E+00	0.00E+00
k1	0.00E+00	1.70E+05
k2	0.00E+00	0.00E+00
k3	0.00E+00	0.00E+00
k4	0.00E+00	0.00E+00
k5	6.69E+04	−1.30E+05
k6	0.00E+00	0.00E+00
k7	−1.06E+05	1.21E+05
k8	7.23E+04	−6.60E+04
k9	−1.39E+04	1.04E+04

The above approach is based on fitting one reference isotherm with a 9th order polynomial as follows.

$$P_{ref} = \sum_{0}^{9} k_i C^i \quad (1)$$

where the parameters of P_{ref}, k_i, and C, are the experimental reference pressure, the fitting parameters and the concentration at the pressure plateau, respectively.

In order to evaluate equilibrium pressure at different temperatures than the reference isotherm T_{ref}, we employ to the Van't Hoff law, obtaining the following relationship:

$$\ln \frac{P}{P_{ref}} = \frac{\Delta H}{R} \left(\frac{1}{T} - \frac{1}{T_{ref}} \right) \quad (2)$$

Thus, the enthalpy of reaction can be calculated from Eq. (3):

$$\Delta H = \frac{R}{(1/T - 1/T_{ref})} \cdot \ln \left(\frac{P}{\sum_{0}^{9} k_i C^i} \right) \quad (3)$$
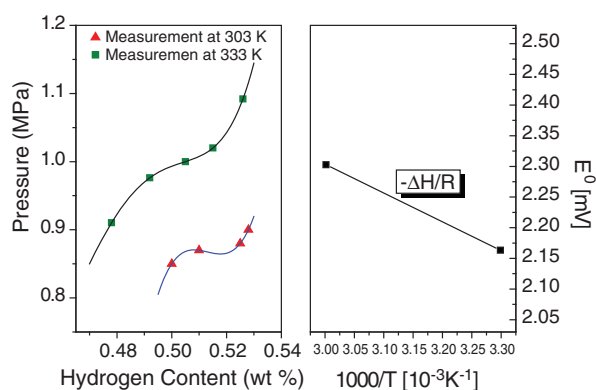
Fig. 15. P-C-T curves and van't Hoff equation diagram of $TiMn_{0.4}Fe_{0.2}V_{0.4}$ (Symbols represent the experimental data while lines are made from the 9th order polynomial approach).

4. CONCLUSIONS

In this work, TiFe-based alloys have been prepared and the Rietveld analysis has revealed that the systems are multiphase. All samples have the characteristic BCC main phase but small amounts of C14 and C15 Laves phases co-exist with the main phase. The BCC phase itself can only absorb a small hydrogen amount, but its hydrogen absorption capacity can be greatly improved by the catalyst of the C14 Laves phase. However, C14 Laves phase should be as a secondary, catalyst phase, otherwise, it has the adverse effect for the maximum hydrogen absorption. The maximum gravimetric density of 4.3 wt%, has been obtained on the sample with the BCC main phase. The presence of Zr favors the formation of the C15 Laves phase, and deteriorates the maximum absorption, since it intercepts the crystallization of the BCC phase. P-C-T curves for absorption have been simulated with a 9th order polynomial fitting, in order to evaluate the enthalpy of reaction ΔH and compare it with the one calculated from the experimental data. There is a good agreement between the simulated and experimental isotherms and the error for the calculation of enthalpy is only 15%.

References and Notes

1. H. Y. Cai, P. Millet, and P. Dantzer, *J. Alloys Comp.* 231, 427 (**1995**).
2. L. Schlapbach and A. Zuttel, *Nature* 414, 353 (**2001**).
3. H.-V. Midden, A. Prodan, E. Zupanič, R. Žitko, S. S. Makridis, and Athanasios K Stubos, *J. Phys. Chem. C* 114, 4221 (**2010**).
4. R. Wiswall, Topics Appl. Phys., edited by G. Alefeld and J. V61kl, Springer, Berlin (**1978**).
5. H. Suzuki, Y. Osumi, A. Kato, K. Oguro, and M. Nakane, *J. Less-Common Met.* 89, 545 (**1983**).
6. S. Ono, Y. Ishido, E. Akiba, K. Jindo, Y. Sawada, I. Kitagawa, and T. Kakutani, *Proceedings 5th World Hydrogen Energy Conference* (**1984**), Vol. 3, p. 1291.
7. O. Bernauer and C. Halene, *J. Less-Common Met.* 131, 213 (**1987**).
8. F. A. Lewis, The Palladium-Hydrogen System, Academic Press, London (**1967**).
9. G. Bronoel, J. Sarradin, M. Bonnemay, and A. Percheron-Guegan, *Int. J. Hydrogen Energy* 1, 251 (**1976**).
10. T. Sakai, K. Oguro, H. Miyamura, N. Kuriyama, A. Kato, H. Ishikawa, and C. Iwakura, *J. Less-Common Met.* 161, 193 (**1990**).
11. C. Jordy, A. Percheron-Guegan, J. Bouet, P. Sanchez, and J. Leonardi, *J. Less-Common Met.* 172, 1236 (**1991**).
12. H. Suda, *Int. J. Hydrogen Energy* 12, 323 (**1987**).
13. M. Ron and Y. Josephy, *J. Phys. Chemie* 164, 1475 (**1989**).
14. N. Nagel, Y. Komazaki, M. Uchida, S. Suda, and Y. Matsubara, *J. Less-Common Met.* 104, 307 (**1984**).
15. C. L. Huffine, Metal Hydrides, edited by W. M. Mueller, J. E Blackledge, and G. G. Libowitz, Academic Press, New York (**1968**).
16. R. Lasser and T. Shoba Hydrogen Storage Materials, Trans. Tech., edited by R. Barnes, Publications, Switzerland (**1988**).
17. J. J. Reilly, A. Holtz, and R. H. Wiswall, *Rev. Sci. Instrum.* 42, 1485 (**1971**).
18. P. M. Golben, in Multistage Hydride-Hydrogen Compressors, *Proceedings 18th Intersociety Energy Conversion Engineering Conference*, 1746 (**1983**).

19. T. Kumano, B. Tada, Y. Tsuchida, Y. Kuraoka, T. Ishige, and H. Baba, *Z. Phys. Chemie* 164, 1509 (**1989**).

20. K. Nasako, T. Yonesaki, K. Sato, T. Imoto, S. Fujitani, N. Hiro, T. Hirose, K. Fukushima, T. Saito, and I. Yonezu, *Z. Phys. Chemie* 183, 235 (**1994**).

21. M. Singh, *Int. J. Hydrogen Energy* 21, 223 (**2007**).

22. G. Srinivas, V. Sankaranarayanan, and S. Ramaprabhu, *J. Alloys Comp.* 448, 159 (**2008**).

23. G. Friedlmeier and M. Groll, *J. Alloys Comp.* 253, 550 (**1997**).

24. J. Paya, M. Linder, and E. Laurien, *Int. J. Hydrogen Energy* 34, 3173 (**2009**).

25. M. Gambini, *Int. J. Hydrogen Energy* 19, 67 (**1994**).

26. J. Paya, M. Linder, and E. Laurien, *J. Alloys Comp.* 484, 190 (**2009**).

27. A. Kinaci and M. K. Aydinol, *Int. J. Hydrogen Energy* 32, 2466 (**2007**).

28. P. Thompson, J. J. Reilly, and J. M. Hastings, *J. Appl. Crystallogr* 22, 256 (**1989**).

29. H. Miao, M. Gao, Y. Liu, Y. Lin, J. Wang, and H. Pan, *Int. J. Hydrogen Energy* 32, 3947 (**2007**).

30. T. Sasai, K. Oku, H. Konno, K. Onouwe, and S. Kashu, *J. Less-Common Met.* 89, 281 (**1983**).

31. T. H. Jang, J. I. Han, and Lee Jai-Young, *J. Less-Common Met.* 119, 237 (**1986**).

32. G. D. Sandrock and P. D. Goodell, *J. Less Common-Met.* 73, 161 (**1980**).

33. S. H. Lim and J.-Y. Lee, *J. Less-Common Met.* 97, 65 (**1984**).

34. N. Rajalakshmi and K. S. Dhathathreyan, *Int. J. Hydrogen Energy* 24, 625 (**1999**).

35. V. Paul-Boncour, *J. Advanced Science* 19, 16 (**2007**).

36. A. Szajek, M. Jurczyk, and E. Jankowska, *J. Alloys Comp.* 348, 285 (**2003**).

37. C. Suryanarayana, *Prog. Mater Sci.* 46, 1 (**2001**).

38. J. S. Benjamin, *Sci. Am.* 40, 234 (**1976**).

39. P. Mandal and O. N. Srivastava, *J. Alloys Comp.* 205, 111 (**1994**).

40. www.rietica.com

41. A. Sarkar, P. Mukherjee, and P. Barat, Rietveld refinement of ZrSiO$_4$: Application of a phenomenological model of anisotropic peak width, Variable Energy Cyclotron Centre, 1/AF Bidhan Nagar, Kolkata 700064, India.

42. J. Payá, M. Linder, E. Laurien, and J. M. Corberán, *J. Alloys Comp.* 484, 190 (**2009**).

RESEARCH ARTICLE